**Proceedings of ASME 2007 International Design Engineering Technical Conferences &
Computers and Information in Engineering Conference
IDETC/CIE 2007
September 4-7, 2007, Las Vegas, Nevada, USA**

DETC2007-35526

AN IMPLICIT TIME-STEPPING METHOD FOR QUASI-RIGID MULTIBODY SYSTEMS WITH INTERMITTENT CONTACT

Nilanjan Chakraborty and Stephen Berard and Srinivas Akella and Jeff Trinkle
Department of Computer Science
Rensselaer Polytechnic Institute
Troy, New York 12180
Email: {chakrn2, sberard, sakella, trink}@cs.rpi.edu

ABSTRACT

We recently developed a time-stepping method for simulating rigid multi-body systems with intermittent contact that is implicit in the geometric information [1]. In this paper, we extend this formulation to quasi-rigid or locally compliant objects, i.e., objects with a rigid core surrounded by a compliant layer, similar to Song et al. [2]. The difference in our compliance model from existing quasi-rigid models is that, based on physical motivations, we assume the compliant layer has a maximum possible normal deflection beyond which it acts as a rigid body. Therefore, we use an extension of the Kelvin-Voigt (i.e. linear spring-damper) model for obtaining the normal contact forces by incorporating the thickness of the compliant layer explicitly in the contact model. We use the Kelvin-Voigt model for the tangential forces and assume that the contact forces and moment satisfy an ellipsoidal friction law.

We model each object as an intersection of convex inequalities and write the contact constraint as a complementarity constraint between the contact force and a distance function dependent on the closest points and the local deformation of the body. The closest points satisfy a system of nonlinear algebraic equations and the resultant continuous model is a Differential Complementarity Problem (DCP). This enables us to formulate a geometrically implicit time-stepping scheme for solving the DCP which is more accurate than a geometrically explicit scheme. The discrete problem to be solved at each time-step is a mixed nonlinear complementarity problem.

INTRODUCTION

To automatically plan and execute tasks involving intermittent contact, one must be able to accurately predict the object motions in such systems. Applications include haptic interactions, collaborative human-robot manipulation, such as rearranging the furniture in a house, as well as industrial automation, such as simulation of parts feeders. These applications are characterized by intermittency of contact, presence of stick-slip frictional behavior and deformation at the contact surfaces. The deformation at the contact is usually very *small* and therefore the objects can be modeled as quasi-rigid or locally compliant [2–5], *i.e.*, each body consists of a rigid core surrounded by a thin compliant shell. Such objects may have a maximum possible deflection and the contact will behave as a rigid contact once the maximum deflection is reached. This motivates us to model the objects as locally compliant objects with a limit on the allowable deflection at the contact.

The dynamics of multi-rigid-body systems with unilateral contacts can be modeled as differential algebraic equations (DAE) [6] if the contact interactions (sliding, rolling, or separating) at each contact are known. However, in general, the contact interactions are not known *a priori*, but rather are discovered as part of the solution process. To handle the many possibilities in a rigorous theoretical and computational framework, the model is formulated as a differential complementarity problem [7, 8]. The primary sources of stability and accuracy problems in dynamic simulation are polyhedral approximations of smooth bodies, the decoupling of collision detection from the solution of the

dynamic time-stepping subproblem, and approximations to the quadratic Coulomb friction model. Irrespective of whether the model of the object is rigid or locally compliant, all state-of-the-art time steppers [4,9,10] are explicit with respect to the geometric information, *i.e.*, they use the geometric information obtained from a collision detection algorithm at the start of the current time step to compute the state at the end of the time step without modifying this information. The method of Tzitzouris [11] is the only geometrically implicit method developed to date, but it requires a closed form distance function between the two bodies which is usually not available. In our previous work [1] we showed simulation results of a disk rolling on a plane without slip and depicted the loss of energy due to polyhedral approximation and the approximation of the distance function. To overcome this, we presented a *geometrically implicit* time-stepping scheme for convex objects described by implicit surfaces in which the collision detection and dynamic time stepping problem is solved in the same time step.

The main focus of this paper is to develop a geometrically-implicit time-stepping model for dynamic simulation of convex objects described by implicit surfaces, assuming single point contact between the objects and local compliance at the contacts. However, unlike other locally compliant models, we assume a limit on the maximum amount of allowable deflection which is realistic in many scenarios (*e.g.*, to model flesh and bone for biomechanics and human robot interaction). We extend our formulation for contact constraints presented in [1] to include the deflection at the contact and use a linear viscoelastic Kelvin-Voigt model (*i.e.*, a linear spring-damper model) for modeling the compliance. The contact constraints also take into account the maximum allowable deflection at the contact point. Since we are assuming an upper bound on the deflection, there can be an instantaneous jump in the contact forces when the rigid core is reached. Thus we formulate our time-stepping problem at the velocity-impulse level instead of the force-acceleration level so that the resulting time-steppers are better behaved.

Our paper is organized as follows. In Section 1, we survey the relevant literature. In Section 2, we present both the continuous and discrete time dynamics model for multi-rigid-body systems with an ellipsoidal dry friction law. In Section 3, we review the non-penetration condition for the contact constraints presented in [1]. Thereafter, in section 4, we modify these contact constraints to include compliant contacts with limits on the maximum allowable deflection. The discrete time dynamics model along with the contact constraints form a mixed nonlinear complementarity problem at each time-step. In Section 5, we give examples that validate and elucidate our time-stepping scheme. Finally in section 6, we present our conclusions and lay out the future work.

RELATED WORK

Dynamics of multi-rigid-body systems with unilateral contacts can be modeled as differential algebraic equations (DAE) [6] if the contact interactions (sliding, rolling, or separating) at each contact are known. However, in general, the contact interactions are not known *a priori*, but rather are discovered as part of the solution process. To handle the many possibilities in a rigorous theoretical and computational framework, the model is formulated as a differential complementarity problem [7, 8]. The differential complementarity problem is solved using a time-stepping scheme and the resultant system of equations to be solved at each step is a (linear/nonlinear) complementarity problem.

Definition 1 (*Nonlinear Complementarity Problem (NCP)*)**.** Let $f(\mathbf{z}) \in \mathbb{R}^n$ be a given vector function of $\mathbf{z} \in \mathbb{R}^n$. The nonlinear complementarity problem is to find $\mathbf{z}$ satisfying $0 \leq \mathbf{z} \perp f(\mathbf{z}) \geq 0$, where the symbol $\perp$ connotes orthogonality (*i.e.*, $f(\mathbf{z}) \cdot \mathbf{z} = 0$) and vector inequalities hold on a per element basis.

When $f(\mathbf{z})$ is linear in $\mathbf{z}$, then the problem is referred to as a linear complementarity problem (LCP). Of particular importance to this work is a generalization of the NCP known as the *mixed nonlinear complementarity problem* [12].

Definition 2. Let $g(\mathbf{u},\mathbf{v}) : \mathbb{R}^{n_1} \times \mathbb{R}^{n_2} \rightarrow \mathbb{R}^{n_1}$ and $f(\mathbf{u},\mathbf{v}) : \mathbb{R}^{n_1} \times \mathbb{R}^{n_2} \rightarrow \mathbb{R}^{n_2}$ be given vector functions of $\mathbf{u} \in \mathbb{R}^{n_1}$ and $\mathbf{v} \in \mathbb{R}^{n_2}$, with $n_1 + n_2 = n$. The mixed nonlinear complementarity problem is to find $\mathbf{u}$ and $\mathbf{v}$ satisfying

$$g(\mathbf{u},\mathbf{v}) = 0, \qquad \mathbf{u}, \text{free}$$
$$0 \leq \mathbf{v} \perp f(\mathbf{u},\mathbf{v}) \geq 0$$

Frictional collisions between rigid bodies have a long history in mechanics [13, 14]. Here, we give an overview of the basic approaches and refer the reader to a recent survey article [15] for a more comprehensive review. There are two primary approaches to modeling collisions: coefficient of restitution based approaches and force based methods. In the former, the process of energy transfer and dissipation during collision is modeled by various coefficients relating the velocity (or impulses) before contact to that after contact. However, the extension of these concepts to situations with multiple contacts is not straightforward. The force based approaches use a compliant contact model to compute the contact forces where the contact compliance is modeled as a (linear/nonlinear) spring-damper system. In the simplest model (known as Kelvin-Voigt model or linear spring-damper model), the normal contact force is given by a linear function of the deformation and the rate of deformation ($F = k\delta + c\dot{\delta}$) *i.e.* the flexibility of the body is lumped as a linear spring (with spring constant k) and damper (with damping coefficient c). The limitations of the linear model are documented in [15]. Hertz introduced a nonlinear model of the form

$F = k\delta^n$, where n is a constant [16]. This model was extended to a nonlinear spring-damper model by Hunt and Crossley [17] of the form $F = k\delta^n + c\delta^p\dot{\delta}^q$, where p,q are constants. The models presented above are believed to be of increasing accuracy but there are more unknown constants dependent on geometry of the objects and material properties that have to be determined experimentally (except for some simple cases). This is a general feature of all proposed contact compliance models. In [18] a continuum model of the deformations at each contact is used. Song and Kumar [2] have used a 3D linear distributed contact model to compute the contact forces. In this paper we use a lumped 3D linear spring-damper to model the contact compliance similar to [19]. However, we note that we could have replaced this with a lumped nonlinear model if required. We use an elliptic dry friction law [20] that is a generalization of Coulomb's friction law to model the friction at the contact.

DYNAMIC MODEL FOR RIGID BODY SYSTEMS

In complementarity methods, the instantaneous equations of motion of a multi-rigid-body system consist of five parts: (a) Newton-Euler equations, (b) Kinematic map relating the generalized velocities to the linear and angular velocities, (c) Equality constraints to model joints, (d) Normal contact condition to model intermittent contact, and (e) Friction law. Parts (a) and (b) form a system of ordinary differential equations, (c) is a system of (nonlinear) algebraic equations, (d) is given by a system of complementarity constraints, and (e) can be written as a system of complementarity constraints for Coulomb friction law using the maximum work dissipation principle. In this paper we use a more general elliptic dry friction law [20]. Thus, the dynamic model is a *differential complementarity problem* (DCP). To solve this system of equations, we set up a time-stepping scheme and solve a complementarity problem at each time step. We present below the instantaneous-time formulation as well as an Euler time-stepping scheme. To simplify the exposition, we ignore the presence of joints or bilateral constraints in the following discussion. However, all of the discussion below holds in the presence of bilateral constraints.

To describe the dynamic model mathematically, we first introduce some notation. Let $\mathbf{q}_j$ be the position and orientation of body j in an inertial frame and ν_j be the concatenated vector of linear ($\mathbf{v}$) and angular (ω) velocities. The generalized coordinates, $\mathbf{q}$, and generalized velocity, ν of the whole system are formed by concatenating $\mathbf{q}_j$ and ν_j respectively. Let λ_{in} be the normal contact force at the ith contact and λ_n be the concatenated vector of the normal contact forces. Let λ_{it} and λ_{io} be the orthogonal components of the friction force on the tangential plane at the ith contact and λ_t, λ_o be the respective concatenated vectors. Let λ_{ir} be the frictional moment about the ith contact normal and λ_r be the concatenated vector of the frictional moments. Let n_b be the number of bodies and n_c be the number of contacts. The instantaneous dynamic model can then be written as follows:

Newton-Euler Equations of Motion:

$$\mathbf{M}(\mathbf{q})\dot{\nu} = \mathbf{W}_n\lambda_n + \mathbf{W}_t\lambda_t + \mathbf{W}_o\lambda_o + \mathbf{W}_r\lambda_r + \lambda_{app} + \lambda_{vp} \qquad (1)$$

where $\mathbf{M}(\mathbf{q})$ is the inertia tensor, λ_{app} is the vector of external forces, λ_{vp} is the vector of Coriolis and centripetal forces, $\mathbf{W}_n$, $\mathbf{W}_t$, $\mathbf{W}_o$, and $\mathbf{W}_r$ are dependent on $\mathbf{q}$ and map the normal contact forces, frictional contact forces, and frictional moments to the body reference frame.

Kinematic Map:

$$\dot{\mathbf{q}} = \mathbf{G}(\mathbf{q})\nu \qquad (2)$$

where $\mathbf{G}$ is the matrix mapping the generalized velocity of the body to the time derivative of the position and orientation. The Jacobian $\mathbf{G}$ may be a non-square matrix (*e.g.*, using a unit quaternion to represent orientation) but $\mathbf{G}^T\mathbf{G} = \mathbf{I}$.

Nonpenetration Constraints: The normal contact constraint for the ith contact is

$$0 \le \lambda_{in} \perp \psi_{in}(\mathbf{q},t) \ge 0 \qquad (3)$$

where $i = 1 \ldots n_c$ are the number of contacts, ψ_{in} is a signed distance function or *gap function* for the ith contact with the property $\psi_{in}(\mathbf{q},t) > 0$ for separation, $\psi_{in}(\mathbf{q},t) = 0$ for touching, and $\psi_{in}(\mathbf{q},t) < 0$ for interpenetration. The above gap function is defined in the configuration space of the system. Note that there is usually no closed form expression for $\psi_{in}(\mathbf{q},t)$.

Friction Model:

$$(\lambda_{it},\ \lambda_{io}),\ \lambda_{ir} \in \operatorname{argmax}\{-(v_{it}\lambda'_{it} + v_{io}\lambda'_{io} + v_{ir}\lambda'_{ir}) \ : \ (\lambda'_{it},\ \lambda'_{io}, \lambda'_{ir}) \in \mathbf{F}_i(\lambda_{in}, \mu_i)\}$$

where $i = 1 \ldots n_c$, $\mathbf{v}_i$ is the relative velocity at contact i and the friction cone is defined by $\mathbf{F}_i(\lambda_{in}, \mu_i) = \{(\lambda_{it},\ \lambda_{io},\ \lambda_{ir}) : \left(\frac{\lambda_{it}}{e_{it}}\right)^2 + \left(\frac{\lambda_{io}}{e_{io}}\right)^2 + \left(\frac{\lambda_{ir}}{e_{ir}}\right)^2 \le \mu_i^2\lambda_{in}^2\}$ where e_{it}, e_{io} and e_{ir} are given positive constants defining the friction ellipsoid and μ_i is the coefficient of friction at the ith contact [21, 22].

Time-Stepping Formulation: We use a velocity-level formulation and an Euler time-stepping scheme to discretize the above system of equations. Let t_ℓ denote the current time, h be the time step. Use the superscripts ℓ and $\ell+1$ to denote quantities at beginning and end of the ℓth time step respectively. Using $\dot{\mathrm{v}}^{\ell+1} \approx (\mathrm{v}^{\ell+1} - \mathrm{v}^{\ell})/h$ and $\dot{\mathbf{q}}^{\ell+1} \approx (\mathbf{q}^{\ell+1} - \mathbf{q}^{\ell})/h$, and writing in terms of the impulses we get the following discrete time system.

$$\begin{aligned}
\mathbf{M}\mathrm{v}^{\ell+1} &= \mathbf{M}\mathrm{v}^{\ell} + h(\mathbf{W}_{\mathrm{n}}\lambda_{\mathrm{n}}^{\ell+1} + \mathbf{W}_{\mathrm{t}}\lambda_{\mathrm{t}}^{\ell+1} + \mathbf{W}_{\mathrm{o}}\lambda_{\mathrm{o}}^{\ell+1} + \mathbf{W}_{\mathrm{r}}\lambda_{\mathrm{r}}^{\ell+1} \\
&\quad + \lambda_{\mathrm{app}}^{\ell} + \lambda_{\mathrm{vp}}) \\
\mathbf{q}^{\ell+1} &= \mathbf{q}^{\ell} + h\mathbf{G}\mathrm{v}^{\ell+1} \\
0 \le h\lambda_{\mathrm{n}}^{\ell+1} &\perp \psi_{\mathrm{n}}(\mathbf{q}^{\ell+1}) \ge 0 \\
h(\lambda_{\mathrm{it}}^{\ell+1},\, \lambda_{\mathrm{io}}^{\ell+1},\, \lambda_{\mathrm{ir}}^{\ell+1}) &\in \mathrm{argmax}\{-(\left(v_{\mathrm{it}}^{\ell+1}\right)\lambda'_{\mathrm{it}} + \left(v_{\mathrm{io}}^{\ell+1}\right)\lambda'_{\mathrm{io}} \\
&\quad + \left(v_{\mathrm{ir}}^{\ell+1}\right)\lambda'_{\mathrm{ir}}) \\
&\quad : h(\lambda_{\mathrm{it}}^{\ell+1},\, \lambda_{\mathrm{io}}^{\ell+1}, \lambda_{\mathrm{ir}}^{\ell+1}) \in \mathbf{F}_i(h\lambda_{\mathrm{in}}, \mu_i)\}
\end{aligned} \tag{4}$$

The argmax formulation of the friction law has a useful alternative formulation [20]:

$$\begin{aligned}
\mathbf{E}_t^2\mathbf{U}\mathbf{p}_{\mathrm{n}} \circ \mathbf{W}_{\mathrm{t}}^T\mathrm{v}^{\ell+1} + \mathbf{p}_{\mathrm{t}} \circ \sigma &= 0 \\
\mathbf{E}_o^2\mathbf{U}\mathbf{p}_{\mathrm{n}} \circ \mathbf{W}_{\mathrm{o}}^T\mathrm{v}^{\ell+1} + \mathbf{p}_{\mathrm{o}} \circ \sigma &= 0 \\
\mathbf{E}_r^2\mathbf{U}\mathbf{p}_{\mathrm{n}} \circ \mathbf{W}_{\mathrm{r}}^T\mathrm{v}^{\ell+1} + \mathbf{p}_{\mathrm{r}} \circ \sigma &= 0 \\
(\mathbf{U}\mathbf{p}_{\mathrm{n}}) \circ (\mathbf{U}\mathbf{p}_{\mathrm{n}}) - \left(\mathbf{E}_{\mathrm{t}}^2\right)^{-1}(\mathbf{p}_{\mathrm{t}} \circ \mathbf{p}_{\mathrm{t}}) - \left(\mathbf{E}_{\mathrm{o}}^2\right)^{-1}(\mathbf{p}_{\mathrm{o}} \circ \mathbf{p}_{\mathrm{o}}) & \\
- \left(\mathbf{E}_{\mathrm{r}}^2\right)^{-1}(\mathbf{p}_{\mathrm{r}} \circ \mathbf{p}_{\mathrm{r}}) \ge 0 &
\end{aligned} \tag{5}$$

where $\circ$ connotes the Hadamard product, the impulse $\mathbf{p}_{(\cdot)} = h\lambda_{(\cdot)}$, the matrices $\mathbf{E}_{\mathrm{t}}$, $\mathbf{E}_{\mathrm{o}}$, $\mathbf{E}_{\mathrm{r}}$, and $\mathbf{U}$ are diagonal with ith diagonal element equal to e_{it}, e_{io}, e_{ir}, and μ_i respectively, σ is a concatenated vector of the Lagrange multipliers arising from the Fritz John optimality conditions of argmax formulation. Each component of σ (σ_i) is the magnitude of the slip velocity at contact i.

Equation 4, which is to be solved at each time step, is either an LCP or an NCP depending on the time of evaluation of $\mathbf{W}_{(\cdot)}$, the approximation used for $\psi_{\mathrm{n}}(\mathbf{q}^{\ell+1})$, and the representation of the friction model. If we evaluate $\mathbf{W}_{(\cdot)}$ at $\ell+1$, use a quadratic friction law (Equation (5)), and use $\psi_{\mathrm{n}}(\mathbf{q}^{\ell+1})$, we have a geometrically implicit NCP formulation ensuring that the contact conditions are satisfied at the end of the time step. However, evaluating $\psi_{\mathrm{n}}(\mathbf{q}^{\ell+1})$ is possible only if we have a closed form expression for the distance function, which we do not have in general. Instead, in the next section we formulate the gap function between the closest points as a set of algebraic equations, and subsequently extend the formulation to include compliance.

NON-PENETRATION CONSTRAINT

In this section we rewrite the contact condition (Equation 3) as a complementarity condition in the work space, combine it with an optimization problem to find the closest points and prove that the resultant system of equations ensures that the contact constraints are satisfied [1]. For ease of exposition, we assume here that each object is a convex object described by a single implicit surface. A more general formulation where each object is described by an intersection of implicit surfaces is given in Appendix A of [1]. Let us consider the ith contact. Let the two objects be defined by convex functions $f(\xi_1) \le 0$ and $g(\xi_2) \le 0$ respectively, where ξ_1 and ξ_2 are the coordinates of points in the two objects. Let $\mathbf{a}_1$ and $\mathbf{a}_2$ be the closest points on the two objects. The equations of the implicit surfaces have the property that for any point $\mathbf{x}$, the point lies inside the object for $f(\mathbf{x}) < 0$, on the object surface for $f(\mathbf{x}) = 0$, and outside the object for $f(\mathbf{x}) > 0$. Thus, we can define the gap function in work space as either $f(\mathbf{a}_2)$ or $g(\mathbf{a}_1)$ and write the complementarity conditions as either one of the following two conditions:

$$\begin{aligned}
0 \le \lambda_{in} &\perp f(\mathbf{a}_2) \ge 0 \\
0 \le \lambda_{in} &\perp g(\mathbf{a}_1) \ge 0
\end{aligned} \tag{6}$$

where $\mathbf{a}_1$ and $\mathbf{a}_2$ are the closest points on object 1 and 2 given by

$$\mathrm{argmin}\ \{\|\xi_1 - \xi_2\|^2 : f(\xi_1) \le 0,\ g(\xi_2) \le 0\} \tag{7}$$

It can be shown easily from the Karush-Kuhn-Tucker (KKT) conditions of Equation 7 that $\mathbf{a}_1$ and $\mathbf{a}_2$ are the solutions of the following system of algebraic equations.

$$\begin{aligned}
\mathbf{a}_1 - \mathbf{a}_2 &= -l_1\nabla f(\mathbf{a}_1) = l_2\nabla g(\mathbf{a}_2) \\
f(\mathbf{a}_1) &= 0 \\
g(\mathbf{a}_2) &= 0
\end{aligned} \tag{8}$$

where l_1 and l_2 are the Lagrange multipliers. The geometric meaning of the first two equations is that the normals to the two surfaces at their closest points are aligned with the line joining the closest points. The solution to Equation 8 gives the closest point when the two objects are separate. However, when $\mathbf{a}_1 = \mathbf{a}_2$, the solution is either the touching point of the two surfaces or a point lying on the intersection curve of the two surfaces. Thus, as written, Equation 8 and 6 do not guarantee non-penetration. However, note that the distinction between touching points and intersecting points, as shown in Figure 1, is that the normals to the two surfaces at the touching points are aligned while it is not so for intersection points. When $\mathbf{a}_1 = \mathbf{a}_2$, we lose the geometric information that the normals at the two points are aligned if we

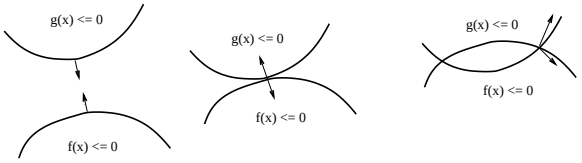

Figure 1. THREE CONTACT CASES: (LEFT) OBJECTS ARE SEPARATE, (MIDDLE) OBJECTS ARE TOUCHING, (RIGHT) OBJECTS ARE INTERSECTING.

write our equations in the form above. Rewriting the above equations in terms of the unit vectors allows us to avoid this problem.

$$\begin{aligned} \mathbf{a}_1 - \mathbf{a}_2 &= -\|\mathbf{a}_1 - \mathbf{a}_2\| \frac{\nabla f(\mathbf{a}_1)}{\|\nabla f(\mathbf{a}_1)\|} \\ \frac{\nabla f(\mathbf{a}_1)}{\|\nabla f(\mathbf{a}_1)\|} &= -\frac{\nabla g(\mathbf{a}_2)}{\|\nabla g(\mathbf{a}_2)\|} \\ f(\mathbf{a}_1) &= 0 \\ g(\mathbf{a}_2) &= 0 \end{aligned} \tag{9}$$

Proposition: *Equation 6 and 9 together represent the contact constraints i.e. the two objects will satisfy the contact constraints at the end of each time step if and only if Equation 6 and 9 hold together.*

Proof: As discussed above.

Note that, since the first two vector equations are equating unit vectors, there are only two independent equations for each, and the above system has 6 independent equations in 6 variables. Although we have restricted our discussion to convex objects, we believe that this framework can be extended to nonconvex objects that are described as an union of convex objects.

COMPLIANT CONTACT MODELING

In this section we describe the 3D linear viscoelastic model of contact [19] and modify our contact constraints to include the deflections at the contact. We incorporate this model in our time-stepping scheme and present the Mixed NCP problem that we are solving at each time step. We extend the Kelvin-Voigt model with the physically motivated observation that the deformations in the normal direction are bounded by some maximum value. For example, a human finger has a thin compliant layer of muscle and tissue surrounding the rigid core (bone). The application of a force on the finger results in a deformation of the thin compliant layer until the rigid core is reached, at which point the non-penetration response is rigid. Therefore, our model allows for a maximum possible deflection, beyond which the contact behaves as a rigid body contact. The linear model can be replaced by a nonlinear model but this comes at the cost of more unknown modeling parameters to be determined experimentally. For simplicity of exposition, we consider only one of the objects to be flexible at each contact. The general formulation where both the bodies are flexible will contain the additional constraint that the contact forces acting on both the bodies have to be equal. For each contact i, the normal impact force λ_{in} is broken apart into two components:

$$\lambda_{in} = \lambda_{inr} + \lambda_{ins} \tag{10}$$

where λ_{ins} is the component of the force that is obtained from the deformation of the spring and λ_{inr} is the component from impact with the rigid core. The tangential force at each contact, $\lambda_{if} = [\lambda_{it}, \lambda_{io}]$ is also given by a linear spring-damper model. However, we do not have a bound on the maximum displacement in the tangential direction. Concatenating all the individual force components into vectors allows us to write for each contact (we drop subscript i for legibility), $\lambda = \mathbf{K}\delta + \mathbf{C}\dot{\delta}$, where $\lambda = [\lambda_{ns}, \lambda_t, \lambda_o]$ and $\delta = [\delta_n, \delta_t, \delta_o]$ are 3×1 column vectors with $\delta_n, \delta_t, \delta_o$ being the normal and tangential deflection. The matrices $\mathbf{K}$, $\mathbf{C}$ are stiffness and damping matrices given by

$$\mathbf{K} = \begin{bmatrix} K_{nn} & K_{nt} & K_{no} \\ K_{tn} & K_{tt} & K_{to} \\ K_{on} & K_{ot} & K_{oo} \end{bmatrix} \qquad \mathbf{C} = \begin{bmatrix} C_{nn} & C_{nt} & C_{no} \\ C_{tn} & C_{tt} & C_{to} \\ C_{on} & C_{ot} & C_{oo} \end{bmatrix}$$

For systems with multiple contact, the contact forces λ, and body deformations δ become concatenations of n_c subvectors, where n_c is the number of contacts. The stiffness and damping matrices are block diagonal matrices of size $3n_c \times 3n_c$, where each diagonal block of size 3×3 represent one contact.

Complementarity Formulation

When we consider contact compliance the contact constraints in Section 3 need to be modified to take into account the deflection δ. We denote the maximum normal deflection by $\delta_n^0 > 0$ and assume that it will be determined experimentally. Figure 2 shows two objects in contact with each other. The bold line shows the deformed shapes of the two objects. The point of contact is the point where the virtual objects shown by dotted lines touch. The deflections of the two objects along the normal at the contact point are δ_{n1} and δ_{n2} respectively. In the subsequent discussion, we will assume $\delta_{n1} = 0$ for simplicity and drop the subscript 2 from δ_{n2}. Therefore, the constraints for the closest points are given by

$$\begin{aligned} \mathbf{a}_1 - \mathbf{a}_2 &= -\|\mathbf{a}_1 - \mathbf{a}_2\| \frac{\nabla f(\mathbf{a}_1)}{\|\nabla f(\mathbf{a}_1)\|} \\ \frac{\nabla f(\mathbf{a}_1)}{\|\nabla f(\mathbf{a}_1)\|} &= -\frac{\nabla g(\mathbf{a}_2)}{\|\nabla g(\mathbf{a}_2)\|} \\ 0 &= f(\mathbf{a}_1) \\ 0 &= g(\mathbf{a}_2) + \bar{\delta}_n \end{aligned} \tag{11}$$

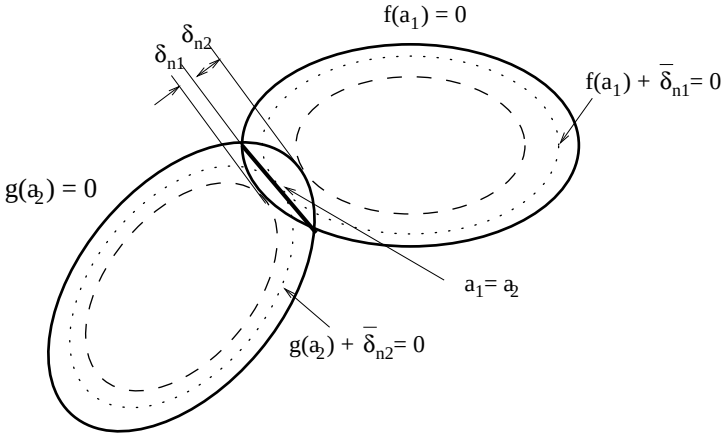

Figure 2. SCHEMATIC REPRESENTATION OF THE DEFLECTION AT CONTACT. THE CONTACT IS WHERE THE DOTTED CURVES TOUCH.

where $\bar{\delta}_n$ is the *algebraic distance*. However, the normal contact force is given in terms of the Euclidean deflection. To obtain the Euclidean deflection from this algebraic deflection we note that the Euclidean deflection is the distance between the point $\mathbf{a}_2$ and the point where the normal to $g(\mathbf{a}_2)+\delta_{n2}=0$ at $\mathbf{a}_2$ intersects $g(\mathbf{a}_2)=0$. From the above argument it can be seen that

$$g(\mathbf{a}_2+\delta_n\frac{\nabla g(\mathbf{a}_2)}{\|\nabla g(\mathbf{a}_2)\|})=0 \tag{12}$$

The complementarity conditions in Equation (6) thus becomes:

$$\begin{aligned} 0 \le \lambda_{ns} \perp \psi(\mathbf{a}_1,\mathbf{a}_2)+\bar{\delta}_n \ge 0 \\ 0 \le \lambda_{nr} \perp \delta_n^o-\delta_n \ge 0 \end{aligned} \tag{13}$$

where $\psi(\mathbf{a}_1,\mathbf{a}_2)=f(\mathbf{a_2})$ or $g(\mathbf{a_1})$ for implicit surfaces. When the two bodies are not in contact the right hand side of both the complementarity constraints are positive and hence we do not have any contact force. The above system of equations are to be written for each of the contacting bodies. This formulation ensures that we satisfy the contact constraints at the end of the time step taking into consideration the possibility of the deflection of the body. It does not require the computation of penetration depth for obtaining the deflection as required in [4]. It ensures that we get a collision response in a fixed time-step scheme.

We can now formulate the mixed NCP for the geometrically-implicit lumped compliant contact time-stepper. The vector of unknowns $\mathbf{z}$ can be partitioned into $\mathbf{z}=[\mathbf{u},\ \mathbf{v}]$ where $\mathbf{u}=[\nu,\ \mathbf{a}_1,\ \mathbf{a}_2,\ \bar{\delta}_n,\ \delta_n,\ \delta_t,\ \delta_o,\ \mathbf{p}_t,\ \mathbf{p}_o,\ \mathbf{p}_r]$ and $\mathbf{v}=[\mathbf{p}_{ns},\ \mathbf{p}_{nr},\ \sigma]$. The equality constraints in the mixed NCP are:

$$\begin{aligned}
0 &= -\mathbf{M}\nu^{\ell+1}+\mathbf{M}\nu^{\ell}+\mathbf{W}_n^{\ell+1}\mathbf{p}_n^{\ell+1}+\mathbf{W}_t^{\ell+1}\mathbf{p}_t^{\ell+1}+\mathbf{W}_o^{\ell+1}\mathbf{p}_o^{\ell+1} \\
&\quad +\mathbf{W}_r^{\ell+1}\mathbf{p}_r^{\ell+1}+\mathbf{p}_{app}^{\ell}+\mathbf{p}_{vp}^{\ell} \\
0 &= \mathbf{p}^{\ell+1}-\left(h\mathbf{K}\delta^{\ell+1}+\mathbf{C}(\delta^{\ell+1}-\delta^{\ell})\right) \\
0 &= (\mathbf{a}_1^{\ell+1}-\mathbf{a}_2^{\ell+1})+\|\mathbf{a}_1^{\ell+1}-\mathbf{a}_2^{\ell+1}\|\frac{\nabla f(\mathbf{a}_1^{\ell+1})}{\|\nabla f(\mathbf{a}_1^{\ell+1})\|} \\
0 &= \frac{\nabla f(\mathbf{a}_1^{\ell+1})}{\|\nabla f(\mathbf{a}_1^{\ell+1})\|}+\frac{\nabla g(\mathbf{a}_2^{\ell+1})}{\|\nabla g(\mathbf{a}_2^{\ell+1})\|} \\
0 &= f(\mathbf{a}_1^{\ell+1}) \\
0 &= g(\mathbf{a}_2^{\ell+1})+\bar{\delta}_n^{\ell+1} \\
0 &= g(\mathbf{a}_2^{\ell+1}+\delta_n^{\ell+1}\frac{\nabla g(\mathbf{a}_2^{\ell+1})}{\|\nabla g(\mathbf{a}_2^{\ell+1})\|}) \\
0 &= \mathbf{E}_t^2\mathbf{U}\mathbf{p}_n^{\ell+1}\circ(\mathbf{W}_t^T)^{\ell+1}\nu^{\ell+1}+\mathbf{p}_t^{\ell+1}\circ\sigma^{\ell+1} \\
0 &= \mathbf{E}_o^2\mathbf{U}\mathbf{p}_n^{\ell+1}\circ(\mathbf{W}_o^T)^{\ell+1}\nu^{\ell+1}+\mathbf{p}_o^{\ell+1}\circ\sigma^{\ell+1} \\
0 &= \mathbf{E}_r^2\mathbf{U}\mathbf{p}_n^{\ell+1}\circ(\mathbf{W}_r^T)^{\ell+1}\nu^{\ell+1}+\mathbf{p}_r^{\ell+1}\circ\sigma^{\ell+1}
\end{aligned} \tag{14}$$

where $\mathbf{p}^{\ell+1}=[\mathbf{p}_n^{\ell+1}\ \mathbf{p}_t^{\ell+1}\ \mathbf{p}_o^{\ell+1}]^T$, $\mathbf{p}_n^{\ell+1}=\mathbf{p}_{ns}^{\ell+1}+\mathbf{p}_{nr}^{\ell+1}$ and $\delta^{\ell+1}=[\delta_n^{\ell+1}\ \delta_t^{\ell+1}\ \delta_o^{\ell+1}]^T$.

The complementarity constraints on $\mathbf{v}$ are:

$$0 \le \begin{bmatrix}\mathbf{p}_{ns}^{\ell+1}\\ \mathbf{p}_{nr}^{\ell+1}\\ \sigma^{\ell+1}\end{bmatrix} \perp \begin{bmatrix}\psi(\mathbf{a}_1^{\ell+1},\ \mathbf{a}_2^{\ell+1})+\bar{\delta}_n^{\ell+1}\\ \delta_n^o-\delta_n^{\ell+1}\\ \zeta/h\end{bmatrix} \ge 0 \tag{15}$$

where

$$\begin{aligned}\zeta &= \mathbf{U}\mathbf{p}_n^{\ell+1}\circ\mathbf{U}\mathbf{p}_n^{\ell+1}-\left(\mathbf{E}_t^2\right)^{-1}\left(\mathbf{p}_t^{\ell+1}\circ\mathbf{p}_t^{\ell+1}\right) \\ &\quad -\left(\mathbf{E}_o^2\right)^{-1}\left(\mathbf{p}_o^{\ell+1}\circ\mathbf{p}_o^{\ell+1}\right)-\left(\mathbf{E}_r^2\right)^{-1}\left(\mathbf{p}_r^{\ell+1}\circ\mathbf{p}_r^{\ell+1}\right)\end{aligned}$$

In the above formulation, we see $u\in\mathbb{R}^{6n_b+13n_c}$, $v\in\mathbb{R}^{3n_c}$, the vector function of equality constraints maps $[u,v]$ to $\mathbb{R}^{6n_b+13n_c}$ and the vector function of complementarity constraints maps $[u,v]$ to $\mathbb{R}^{3n_c}$ where n_b and n_c are the number of bodies and number of contacts respectively. If using convex bodies only, the number of contacts can be determined directly from the number of bodies, $n_c=\sum_{i=1}^{n_b} i$. Lastly, we divide the impulses in Equation 15 by h for numerical stability.

ILLUSTRATIVE EXAMPLES

We present two examples to illustrate our approach. The first example is that of a disc falling onto a elastic half plane

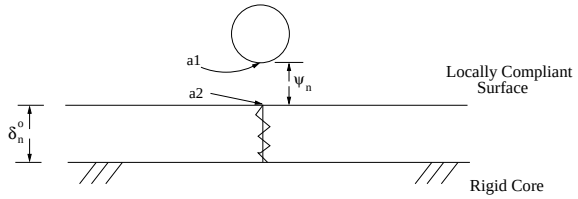

Figure 3. UNIT DISC FALLING ONTO A FRICTIONLESS COMPLIANT SURFACE WITH A SINGLE SPRING ELEMENT.

from rest. We vary the maximum deflection and show that the response when the rigid core is hit is quite different from the one when it is not hit. The second example consists of a rigid spinning ellipsoid dropping on an elastic half plane. We note that the algebraic distance is same as the euclidean distance for a halfplane $\mathbf{a}^t\mathbf{x}+b <= 0$ when $\mathbf{a}$ is a unit vector. Therefore in our presentation of the examples we have not made a distinction between the two. All of our numerical results were obtained by the PATH solver [23]. PATH is freely available and is the most robust complementarity problem solvers available.

Example 1: Unit Disc Falling on a Frictionless Half-Plane

In this example, we simulate a rigid unit disc falling onto a compliant horizontal half-plane. The contact is modeled as a single frictionless contact with no damping. Depending on the value of maximum deflection, the disc may or may not make contact with the rigid core of the half-plane. Figure 3 illustrates the problem.

There are 10 unknowns in this system, with 2 complementarity constraints: $\mathbf{z} = [\mathbf{u},\mathbf{v}] = [v_x, v_y, \omega, \mathbf{a}_{1_x}, \mathbf{a}_{1_y}, \mathbf{a}_{2_x}, \mathbf{a}_{2_y}, \delta_n, p_{\rm ns}, p_{\rm nr}]$. We can formulate the 8 equality constraint equations on $\mathbf{u}$ as (omitted superscripts indicate time l):

$$0 = -\mathbf{M}\mathrm{v}^{\ell+1} + \mathbf{M}\mathrm{v} + \mathbf{W}_{\rm n}^{\ell+1} p_{\rm ns}^{\ell+1} + \mathbf{W}_{\rm n}^{\ell+1} p_{\rm nr}^{\ell+1} + \mathbf{p}_{\rm app} \quad (16)$$

$$0 = p_{\rm ns}^{\ell+1} - hk\delta_n^{\ell+1} \quad (17)$$

$$0 = \mathbf{a}_2^{\ell+1} - \mathbf{a}_1^{\ell+1} + \|\mathbf{a}_2^{\ell+1} - \mathbf{a}_1^{\ell+1}\|\hat{\mathbf{n}} \quad (18)$$

$$0 = \frac{\nabla_{\mathbf{a}_1} f_1(\mathbf{a}_1)^{\ell+1}}{\|\nabla_{\mathbf{a}_1} f_1(\mathbf{a}_1)^{\ell+1}\|} + \hat{\mathbf{n}} \quad (19)$$

$$0 = f_1(\mathbf{a}_1)^{\ell+1} \quad (20)$$

$$0 = f_2(\mathbf{a}_2)^{\ell+1} + \delta_{\rm n}^{\ell+1} \quad (21)$$

The complementarity constraints on $\mathbf{v}$ are:

$$0 \le \begin{bmatrix} p_{\rm ns}^{\ell+1} \\ p_{\rm nr}^{\ell+1} \end{bmatrix} \perp \begin{bmatrix} a_{1_y}^{\ell+1} + \delta_{\rm n}^{\ell+1} \\ \delta_{\rm n}^{o} - \delta_{\rm n}^{\ell+1} \end{bmatrix} \ge 0 \quad (22)$$

The unit disc's initial position was $\mathbf{q} = [0,\ 1.5, 0]$ with zero initial velocity $\mathrm{v} = [0,\ 0,\ 0]$. The only force acting on the disc was gravity. The mass of the disc was 1kg and the moment of inertia about the center of mass was 0.5 kg$\cdot$ m^2. We used a step size $h = 10^{-4}$s. The spring stiffness we used was $k = 1000$kg/s^2. The maximum penetration depth was altered for two experiments such that for the first experiment impact with the rigid core occurs, and for the second experiment impact with the rigid core does not occur. For experiment one, $\delta_n^0 = 0.05$m and for experiment two $\delta_n^0 = 1$m.

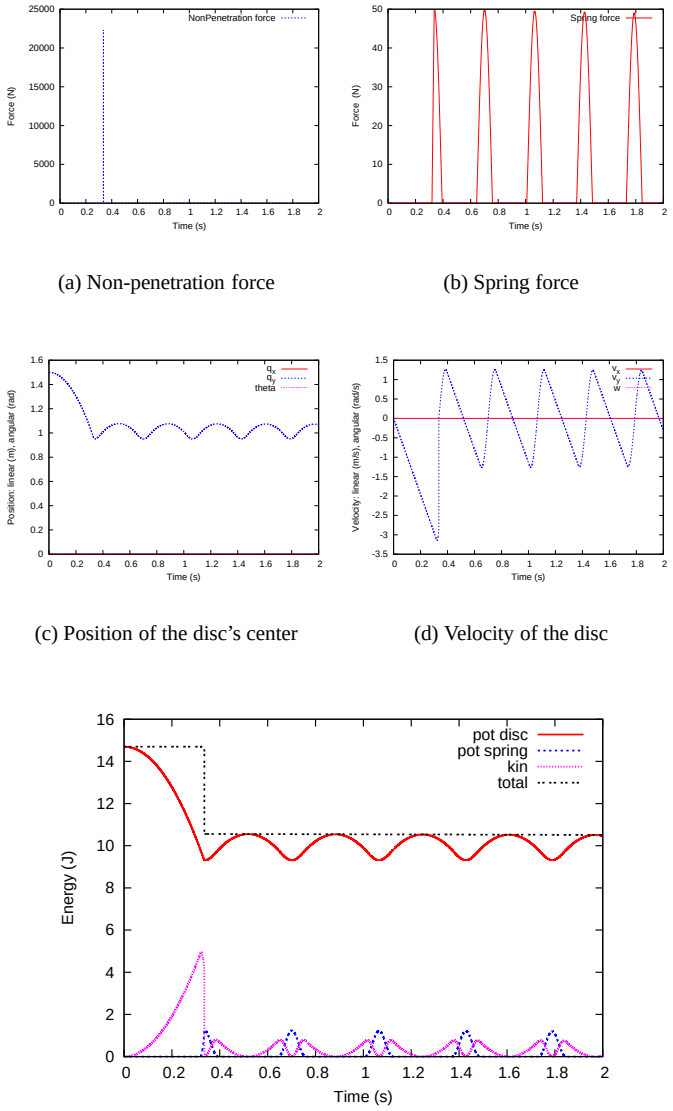

(a) Non-penetration force

(b) Spring force

(c) Position of the disc's center

(d) Velocity of the disc

(e) Energy

Figure 4. SIMULATION RESULTS FOR A UNIT DISC FALLING ON A HALF-PLANE MAKING CONTACT WITH THE RIGID CORE.

Figure 4 illustrates the results of the first experiment in which the maximum spring deflection was not large enough to prevent impact with the rigid core. There is a large non-penetration impulse (Fig. 4(a)) generated at approximately 0.34 seconds corresponding to when the spring reached maximum deflection and impact with the rigid core occurs. As expected with a rigid impact, we also see an instantaneous change in velocity (Fig. 4(d)) to zero and loss of energy (Fig. 4(e)). Subsequent to the impact, the motion of the disc (Fig. 4(c)) become oscillatory as it bounces on the undamped spring (Fig. 4(b)) and the velocity is smooth. The total energy is preserved after impact. The small loss of energy seen in Figure 4(e) is on the order of 10^{-5}J per time step, which is acceptable using a time step of 10^{-4}s and an Euler approximation in the time-stepping formulation. For the second round of experiments, the maximum spring deflection was set large enough that impact with the rigid core never occurs. We see the oscillatory behavior of the position over the lifetime of the simulation (Fig. 5(c)) as expected with an undamped spring. As guaranteed by our model, no component of the normal force comes from impact with the rigid core; the spring contributes solely to the normal force (Fig. 5(b)). Additionally, without any impacts the plot of velocity is smooth with changes occurring only from the force of gravity and the spring force (Fig. 5(d)). Since there is no impact nor damping of the spring, we expect there to be no loss of energy in the system. Figure 5(a) confirms this assumption, where again, the small loss is on the order of 10^{-5}J per step.

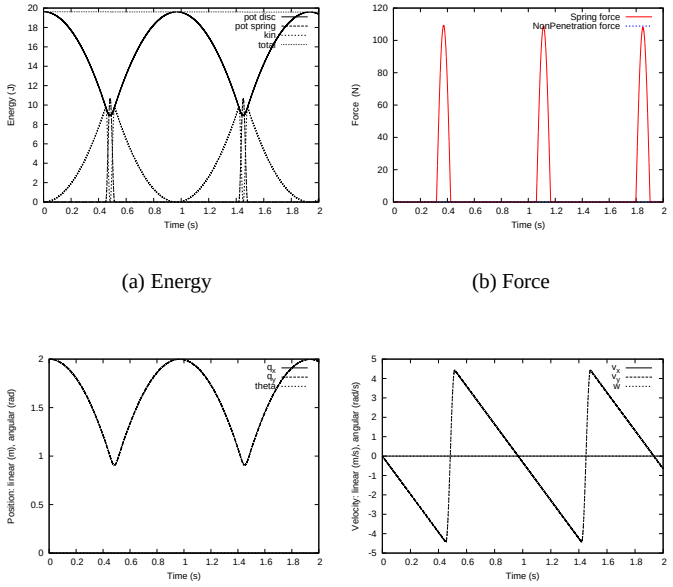

(a) Energy (b) Force

(c) Position (d) Velocity

Figure 5. SIMULATION RESULTS FOR A UNIT DISC FALLING ON A HALF-PLANE NOT MAKING CONTACT WITH THE RIGID CORE.

Example 2: 3D Frictional Ellipsoid

In this example we drop an ellipsoid with an initial angular velocity onto a half-plane. There is no closed form distance function between an ellipsoid and half-plane, and the closest points between the two bodies are found explicitly by our formulation. The minor axes of the ellipsoid are 0.01m and the major axis is 0.5m resulting in the following implicit function describing the surface:

$$f(x,y,z) = \frac{(x-q_x)^2}{0.25^2} + \frac{(y-q_y)^2}{0.005^2} + \frac{(z-q_z)^2}{0.005^2} - 1$$

where $[q_x,\ q_y,\ q_z]$ is the position of the center of gravity of the ellipsoid in the fixed spatial frame. The mass of the ellipsoid is 1.0kg. It has an initial linear velocity of zero and angular velocity of $[0,\ 0,\ 5]^T$ rad/s. For all experiments the only applied force was gravity and we used a step size of 10^{-4} seconds.

Unlike the previous 2D example, the contact in this example is frictional and includes damping of the spring forces. The stiffness K and damping C matrices are:

$$K = \begin{bmatrix} 36000 & 0 & 0 \\ 0 & 8000 & 0 \\ 0 & 0 & 8000 \end{bmatrix} \qquad C = 2\sqrt{K}$$

The friction parameters are: $e_t = 1$, $e_o = 1$, $e_r = 0.04$ and $\mu = 0.4$. The maximum depth was set to $\delta_n^0 = 0.005$m.

We varied the initial orientation of the ellipsoid for two different experiments. In the first experiment we set the initial orientation of the body frame to coincide with the fixed spatial frame $\mathbf{q} = [0,\ 0,\ 0.15, 1,\ 0,\ 0, 0]$, where the first three elements correspond to the ellipsoid's center of gravity and the last four are the unit quaternion representing the orientation. In the second experiment, we angled the initial orientation of the body frame $\mathbf{q} = [0,\ 0,\ 0.15, 0.9962,\ 0,\ 0.0872, 0]$

For the first experiment, we would expect the ellipsoid to have a constant angular velocity while falling, hit the halfplane, and stop spinning due to the torsional friction. We see this exact behavior as shown in Figure 6. There is a large non-penetration impulse occurring just before 0.2 seconds, corresponding to the impact of the ellipsoid on the half-plane. This impact removes most of the energy because of the non-penetration and damping impulses. Corresponding to the rigid impact, there is an instantaneous drop in the angular velocity. The remaining velocity and kinetic energy are slowly dissipated by the torsional friction, and at approximately 0.4 seconds the ellipsoid transitions from sliding to sticking. Unlike the undamped example with the oscillatory behavior of the position, in this example the damping

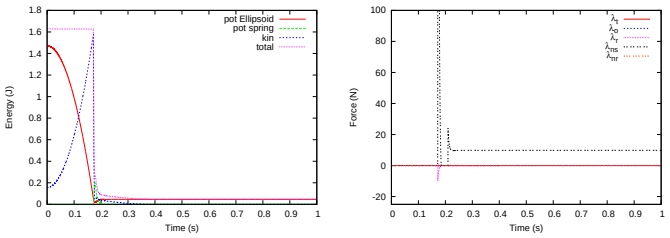

(a) Energy

(b) Force

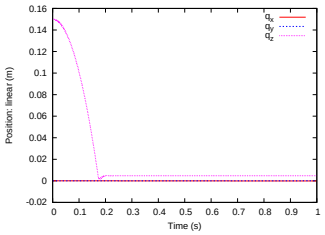

(c) Position

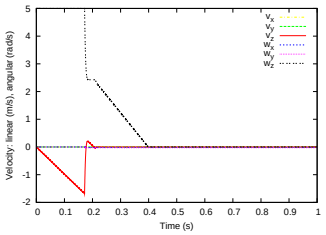

(d) Velocity

Figure 6. SIMULATION RESULTS FOR AN ELLIPSOID DROPPED ONTO A HALFPLANE. Y-AXIS SET TO $[-25, 100]$ IN FORCE PLOT.

causes the position of the ellipsoid to settle to a resting height on the surface. After settling there is a constant normal spring force approximately equal to the weight of the ellipsoid.

In the second experiment, the angled initial orientation causes moments at the time of impact such that angular velocities in the *x* and *y* directions appear after impact. This behavior is seen in our simulation and the results are presented in Figure 7. There again is the large non-penetration impulse generated from hitting the rigid core, however, in this example the impact causes sliding to occur until approximately 0.5 seconds when the ellipsoid transitions to rolling. Since we are using an exact representation of the surface geometry, the rolling behavior continues ad-infinitum as expected.

CONCLUSION

In this paper we presented a geometrically implicit time stepping scheme for dynamic simulation of convex objects with compliant contact, building on our recent work in [1]. We assumed that the objects are described by implicit surfaces and the deflections at the contacts are small. We model the contact compliance using a 3D linear viscoelastic model and motivated by practical applications we explicitly considered a maximum bound on the amount of deflection in our model. We demonstrated our approach through example simulations. We see several directions for future work. We would like to address the question of existence and uniqueness of solutions of the mixed NCP we formulate. In parallel, we wish to perform more extensive numerical experimentation with this approach. Moreover, we want to extend our present approach to non-convex objects described as a union of convex objects. We also plan to extend our approach to objects described by parametric surfaces. Finally, we will incorporate a distributed compliant impact law to simulate a broader class of problems.

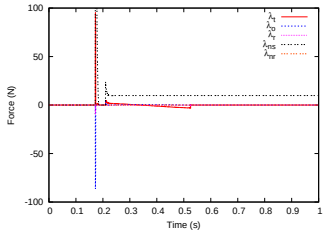

(a) Force

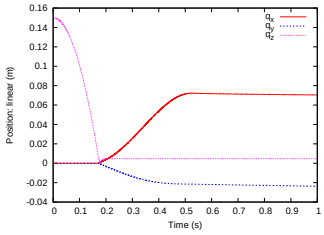

(b) Position

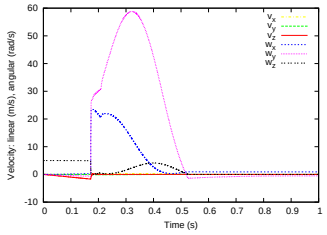

(c) Velocity

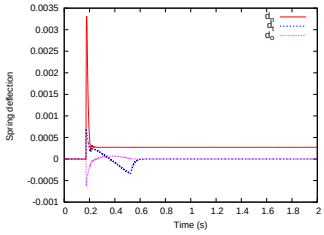

(d) Spring displacements

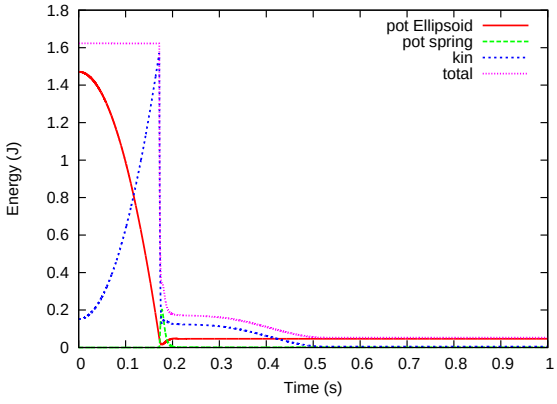

(e) Energy

Figure 7. SIMULATION RESULTS FOR AN ELLIPSOID WITH ANGLED ORIENTATION DROPPED ONTO A HALFPLANE. Y-AXIS SET TO $[-100, 100]$ IN FORCE PLOT.

ACKNOWLEDGMENT

We wish to thank Todd Munson for his insightful discussions on NCPs. This work was supported by the National Science Foundation under grants IIS-0093233, 0139701 (DMS-FRG), 0413227 (IIS-RCV), and 0420703 (MRI). Any opinions, findings, and conclusions or recommendations expressed in this material are those of the author(s) and do not necessarily reflect the views of the National Science Foundation.

REFERENCES

[1] Chakraborty, N., Berard, S., Akella, S., and Trinkle, J. C., 2007. "An implicit time-stepping method for multibody systems with intermittent contact". In Robotics Science and Systems.

[2] Song, P., and Kumar, V., 2003. "Distributed compliant model for efficient dynamic simulation of systems with frictional contacts". In ASME Design Engineering Technical Conferences and Computers and Information in Engineering Conference.

[3] Song, P., Kraus, P., Kumar, V., and Dupont, P., 2001. "Analysis of rigid-body dynamic models for simulation of systems with frictional contacts". *ASME Journal of Applied Mechanics,* **68**(1), pp. 118–128.

[4] Song, P., Pang, J.-S., and Kumar, V., 2004. "A semi-implicit time-stepping model for frictional compliant contact problems". *International Journal for Numerical Methods in Engineering,* **60**, pp. 2231–2261.

[5] Pauly, M., Pai, D. K., and Guibas, L. J., 2004. "Quasi-rigid objects in contact". In ACM SIGGRAPH/Eurographics Symposium on Computer Animation.

[6] Haug, E. J., Wu, S. C., and Yang, S. M., 1986. "Dynamics of mechanical systems with Coulomb friction, stiction, impact and constraint addition-deletion theory". *Mechanism and Machine Theory,* **21**, pp. 365–446.

[7] Cottle, R. W., Pang, J., and Stone, R. E., 1992. *The Linear Complementarity Problem*. Academic Press.

[8] Trinkle, J., Pang, J., Sudarsky, S., and Lo., G., 1997. "On dynamic multi-rigid-body contact problems with Coulomb friction". *Zeitschrift für Angewandte Mathematik und Mechanik,* **77**(4), pp. 267–279.

[9] Stewart, D., and Trinkle, J., 1996. "An implicit time-stepping scheme for rigid body dynamics with inelastic collisions and Coulomb friction". *International Journal of Numerical Methods in Engineering,* **39**, pp. 2673–2691.

[10] Liu, T., and Wang, M. Y., 2005. "Computation of three-dimensional rigid-body dynamics with multiple unilateral contacts using time-stepping and gauss-seidel methods". *Transactions on Automation Science and Engineering,* **2**(1), January, pp. 19–31.

[11] Tzitzouris, J., 2001. "Numerical resolution of frictional multi-rigid-body systems via fully implicit time-stepping and nonlinear complementarity". PhD thesis, The John Hopkins Univerisy.

[12] Pang, J.-S., and Facchinei, F., 2003. *Finite-Dimensional Variational Inequalities and complementarity Problems (I)*. Springer Verlag, New York.

[13] Routh, E. T., 1905. *Dynamics of a System of Rigid Bodies*. Macmillan & Co.

[14] Keller, J. B., 1986. "Impact with friction". *ASME Journal of Applied Mechanics,* **53**, March, pp. 1–4.

[15] Gilardi, G., and Sharif, I., 2002. "Literature survey of contact dynamics modeling". *Mechanism and Machine Theory,* **39**, October, pp. 1213–1239.

[16] Johnson, K. L., 1985. *Contact Mechanics*. Cambridge University Press.

[17] Hunt, K. H., and Crossley, F. R. E., 1975. "Coefficient of restitution interpreted as damping in vibroimpact". *Journal of Applied Mechanics,* **42**, Series E, pp. 440–445.

[18] Wang, Y. T., and Kumar, V., 1994. "Simulation of mechanical systems with unilateral constraints". *ASME Journal of Mechanical Design,* **116**(2), pp. 571–580.

[19] Kraus, P. R., Fredriksson, A., and Kumar, V., 1997. "Modeling of frictional contacts for dynamic simulation". In Proceedings of IROS 1997 Workshop on Dynamic Simulation: Methods and Applications.

[20] Trinkle, J. C., Tzitzouris, J., and Pang, J. S., 2001. "Dynamic multi-rigid-body systems with concurrent distributed contacts: Theory and examples". *Philosophical Transactions on Mathematical, Physical, and Engineering Sciences, Series A,* **359**(1789), December, pp. 2575–2593.

[21] Trinkle, J. C., and Pang, J., 1997. "Dynamic multi-rigid-body systems with concurrent distributed contacts". In IEEE Conference on Robotics and Automation, pp. 2276–2281.

[22] Howe, R. D., and Cutkosky, M. R., 1996. "Practical force-motion models for sliding manipulation.". *International Journal of Robotics Research,* **15**(6), pp. 557–572.

[23] Ferris, M. C., and Munson, T. S., 1998. Complementarity problems in GAMS and the PATH solver. Tech. Rep. MP-TR-1998-12.